Crystalline, microporous zirconium silicates with MFI structure

Bhavana Rakshe, Veda Ramaswamy, S.G. Hegde, R. Vetrivel and A.V. Ramaswamy *

Catalysis Division, National Chemical Laboratory, Pune 411 008, India
E-mail: avr@ncl.ernet.in

Received 5 June 1996; accepted 7 February 1997

Zirconium-containing medium-pore, Al-free molecular sieves (Si/Zr molar ratios > 50) with MFI structure have been synthesized both in alkaline and HF/CH_3NH_2 medium. The samples synthesized in HF/CH_3NH_2 medium exhibit a high crystallinity, bigger particle size, lower surface area and lower catalytic activity in the hydroxylation of phenol as compared to those synthesized in alkaline medium. An expansion in unit cell volume (XRD), an absorption at 965 cm^{-1} (FTIR) and at 212 nm (UV–Visible) as well as the catalytic activity data indicate that upto 0.6 zirconium atom per unit cell (Si/Zr = 158) could be substituted isomorphously within the silicalite-1 framework. The IR study of adsorbed pyridine has shown that strong Lewis acid and weak Brønsted acid sites exist on all zirconium silicate samples, synthesized in alkaline medium. The relative stability of cluster models representing various possible lattice structures and the ordering of molecular orbitals derived from extended Hückel molecular orbital calculations are discussed to understand the nature of active sites in the zirconium silicates.

Keywords: zirconium silicates, MFI structure, synthesis, characterization, EHMO calculations, phenol hydroxylation

1. Introduction

The isomorphous substitution of Si^{4+} by other tetravalent metal ions such as Ti^{4+}, Sn^{4+}, etc. in MFI and MEL structures has led to the invention of selective oxidation catalysts [1–4]. The substitution of silicon by zirconium in the framework of ZSM-5 (MFI) by hydrothermal synthesis has also been attempted but not really substantiated by experimental evidence [5–9]. Costantini et al. have claimed that the synthesis of zirconium silicates is possible in the presence of HF/CH_3NH_2 mineralizer [10]. The effect of Na_2O/SiO_2 and SiO_2/ZrO_2 molar ratios on the synthesis of Zr[ZSM-5] zeolites and their catalytic properties in phenol hydroxylation has also been studied [11]. In this communication, we report the synthesis of crystalline and microporous Al-free zirconium silicates with MFI structure, using $ZrCl_4$ as a precursor in alkaline as well as in HF/CH_3NH_2 medium for comparison. The characterization of structural and catalytic properties elucidates the presence of zirconium in the MFI framework as indicated from the results of XRD, framework FTIR, DR UV–Vis and ^{29}Si MAS NMR spectroscopic techniques as well as by their catalytic activity in the hydroxylation of phenol, using hydrogen peroxide as oxidant.

2. Experimental

2.1. Synthesis

The hydrothermal synthesis of zirconium silicates (Zr-Sil-1) with MFI structure was carried out using the following molar composition of the gel: $1.0SiO_2{:}xZrO_2{:}0.5TPAOH{:}30H_2O$, where $x = 0.0033$–0.02. In a typical synthesis, 0.08 g of $ZrCl_4$ (Merck, 99%) in 5 g of distilled water was added to 21.25 g of tetraethyl orthosilicate (TEOS) (Aldrich, 98%) under slow stirring. After 15–20 min, 50.84 g of tetrapropylammonium hydroxide (TPAOH) (Aldrich, 20% aqueous) was added dropwise. The stirring was continued for 1 h. The remaining volume (8.0 g) of water was added and the resulting mixture was stirred for further 30 min to get a homogeneous clear gel (pH = 12.25) and was transferred to a stainless steel autoclave. The crystallization was conducted at 433 K for 48 h, under static conditions. After the crystallization, the solid product was filtered, washed with deionized water, dried at 383 K and calcined in air at 823 K for 16 h. The product yield was 85 wt%. Four such samples with different Si/Zr ratios, viz. 300, 200, 100 and 50, were prepared and the samples are designated as A to D, respectively. All Zr- Sil-1 samples were treated with 1 M ammonium acetate solution to remove alkali metal impurities, if any and then further calcined at 773 K in air for 8 h. For comparison, a silicalite-1 (Sil-1) sample and a Zr-impregnated silicalite-1 sample were prepared. The latter was made by impregnating Sil-1 with $ZrCl_4$ aqueous solution and then calcining at 773 K. An amorphous Zr-silica sample (Si/Zr = 158) was also prepared from the precursor gel solution which was not subjected to autoclaving and crystallization.

The hydrothermal synthesis of Zr-Sil-1 samples was carried out in HF/CH_3NH_2 medium using the following molar composition of the gel: $1.0SiO_2{:}xZrO_2{:}0.5TPABr{:}3.0F{:}10.0CH_3NH_2{:}70H_2O$, where $x = 0.005$–0.02; TPABr = tetrapropylammonium bromide. In a typical synthesis, 0.23 g of $ZrCl_4$ in 5 g of distilled water was added to a solution containing 6.0 g of fumed silica

* To whom correspondence should be addressed.

(Sigma, 99%) and 30 g of water. After stirring for 30 min, 13.2 g of TPABr in 20 g of water and 11 g of HF (40% aqueous) in 10 g of water were added. The stirring was continued for 1 h and then, 50 g of methylamine (CH_3NH_2) (40% aqueous) was added dropwise to the reaction mixture. Finally, 10 g of water was added and the mixture was stirred for 30 min. Before subjecting the gel to crystallization, 1–2 wt% MFI seeds were added to decrease the crystallization time. The milky gel (pH = 11.0) was transferred to a Teflon-lined steel autoclave. The crystallization was carried out at 473 K for 5 h. After the crystallization, the solid product was filtered, washed and dried at 383 K and calcined in air at 823 K for 16 h. The product yield was 75 wt%. Three such samples having different Si/Zr ratios, viz. 200, 100 and 50, were prepared and the samples were designated as E to G, respectively. The physico-chemical properties of Zr-Sil-1 samples A to G are listed in table 1.

2.2. Characterization

Powder X-ray diffraction patterns of the calcined Zr-Sil-1 samples were obtained on a Rigaku diffractometer (model D-MAX III VC), using Ni-filtered Cu Kα radiation ($\lambda = 1.5406$Å) and a graphite crystal monochromator. The patterns were recorded at a scan rate of 1°/min, using Si as an internal standard. The unit cell parameters were calculated from the corrected d values and refined by using least-squares fitting. Scanning electron micrographs were obtained using a Leica Stereoscan 440 scanning electron microscope. The framework IR spectra were recorded in the mid framework region (1300–400 cm^{-1}) in a 60 SXB Nicolet FTIR spectrophotometer. For the study of surface acid sites, in situ IR spectra were recorded in the hydroxyl region (4000–3000 cm^{-1}), using self-supported wafers which were outgassed in vacuo ($P = 1.33 \times 10^{-4}$ Pa) at 673 K and cooled to 323 K. Then these wafers were equilibrated with 0.7 kPa of pyridine for 1 h. All spectra were run at a resolution of 4 cm^{-1}, after evacuation of the wafers at 373–573 K.

The extent of interaction of orbitals in pyridine and zirconium silicate was measured by the magnitude of the one-electron energy level splitting predicted by extended Hückel molecular orbital calculations. DR UV–Visible spectra were recorded on a Shimadzu spectrophotometer (model UV–VIS 2101 PC). The ^{29}Si MAS NMR spectra of the Zr-silicate samples were obtained at room temperature on a Bruker 300 MHz instrument. The elemental analyses were performed using an ICP spectrometer (TJA Atomscan-25). The surface chemical composition of the Zr-Sil-1 samples was studied with a V.G. Scientific ESCA 3, MK II X-ray photoelectron spectrometer. The binding energy values were corrected for charge effects with reference to the carbon peak at 285.0 eV. The surface area measurements were done on a 100CX Omnisorp system (Coulter) at liquid-nitrogen temperature. The uptake of molecules viz., water, *n*-hexane and cyclohexane, adsorbed over the calcined samples was measured gravimetrically ($p/p_0 = 0.5$) at 293 K on a Cahn (2000G) electrobalance. Calcination in order to decompose the template (TPAOH) was monitored by thermogravimetry and differential thermal analysis (Setaram TG/DTA-92).

2.3. Catalytic reaction

The hydroxylation of phenol was carried out, using aqueous H_2O_2 (30 wt%). In a standard run, 5 g of phenol, 10 g of water and 0.5 g of catalyst were taken in a 50 ml glass reactor and heated to 353 K in an oil bath. 2.13 g H_2O_2 (phenol/H_2O_2 mole ratio = 3) was added to the reaction mixture and the reaction continued for 10 h. The products were analyzed by GC (HP-5880A) equipped with methyl-silicon gum capillary column and a flame ionization detector.

Table 1
Physico-chemical properties of Zr-Sil-1 samples

Sample	Si/Zr [a]	Zr/uc [b]	UCV (Å^3)	ν_{T-O-T} (cm^{-1})	Sorption mass (wt%) [c]			Surface area (m^2/g)	Micropore volume (ml/g)
					water	cyclohexane	*n*-hexane		
silicalite-1	–	–	5321	1100	4.8	4.0	12.5	291	0.16
A	300	0.27	5338	1108	8.0	4.1	13.0	436	0.18
B	200	0.51	5339	1107	7.3	6.8	13.3	386	0.16
C	100	0.61	5342	1103	6.9	4.0	12.8	391	0.17
D	50	0.91	5323	1101	9.1	7.4	14.0	433	0.18
E [d]	200	0.42	5338	1106	7.0	6.2	13.4	265	0.16
F [d]	100	0.60	5340	1101	7.2	4.5	12.9	259	0.17
G [d]	50	0.83	5341	1100	8.5	7.0	13.6	257	0.18

[a] Si/Zr molar input ratio of the gel.
[b] Total amount (molar output of Zr) in the product per unit cell.
[c] Gravimetric adsorption at $p/p_0 = 0.5$ and at 298 K.
[d] Samples synthesized in HF/CH_3NH_2 medium.

3. Results and discussion

3.1. Characterization

Figure 1 shows XRD profiles of the calcined Sil-1 (curve a) and Zr-Sil-1 samples A to D (curves b to e, respectively). All Zr-Sil-1 samples exhibit a high crystallinity, without any impurity phase. The XRD profiles of Zr-Sil-1 are found to be similar to that of Sil-1 and sample F (curve f), except that they do not undergo symmetry change (orthorhombic to monoclinic), on calcination in air at 773 K. The interplanar *d* spacings of silicalite-1 shift to higher values due to the incorporation of the larger zirconium ions (Shannon ionic radii: $Si^{4+} = 0.26$ Å and $Zr^{4+} = 0.59$ Å) [12]. There is an increase in unit cell volume (UCV) from 5321 to 5342 Å^3 with decrease in Si/Zr molar ratio (table 1). It is reasonable to consider that this expansion in UCV corresponds to isomorphous substitution of zirconium in the silicalite framework. The inset in figure 1 compares the experimental UCV with that calculated assuming replacement of Si^{4+} by Zr^{4+} in tetrahedral positions. A very good agreement between the two, within the experimental errors (shown by error bars) up to a metal concentration (x) of 0.0063 (Si/Zr = 158) is observed. But in the case of the Zr-Sil-1 sample (D), the UCV is equal to that of the Sil-1 sample which may be due to the presence of extraframework zirconium, at higher concentration of zirconium. It suggests that only a small amount of zirconium (0.6 atom/uc) can be incorporated with a uniform distribution within the MFI framework due to its larger size. SEM confirms the absence of any amorphous material around Zr-Sil-1 crystals (figure 2). The particle size of Sil-1 sample is about 3–5 μm while Zr-Sil-1 samples A to D are much smaller (0.2–0.5 μm) and are cuboid crystals of uniform morphology. However, the samples E to G, synthesized in HF/CH_3NH_2 medium, form much larger particles (10–15 μm) and their morphology is similar to that of a typical ZSM-5 structure. The typical SEM photographs of the representative samples are shown in figure 2.

The framework FTIR spectra (figure 3) show a shoulder (sh) at about 965 cm^{-1} which may be attributed to Si–O–Zr asymmetric stretching vibrations (ν_{as}), from the possible substitution of Zr^{4+} in the Si–O–Si linkages [13]. However, no such absorption was observed in sample F, Zr-impregnated Sil-1 or amorphous Zr-silica. A similar band near 960 cm^{-1} has been reported for the SiO_2/TiO_2 and titanium silicates (TS-1 and TS-2) typically representing the asymmetric stretching vibrations of Si–O–Ti linkages [14–17]. For well dispersed zirconia on silica, Dang et al. [18] have observed a band at 945 cm^{-1} from difference IR spectra and attributed this vibration to the possible formation of Si–O–Zr linkages in their samples. Additionally, a band (sh) at 877 cm^{-1} was observed probably due to stretching vibrations (ν_s) of Zr=O species for higher Zr content (sample C) [19,20]. A nearly linear decrease in the position of the main T–O–T vibrations (ν_{as}) at about 1100 cm^{-1} is observed (table 1) with increasing Zr content in the MFI framework [13].

In figure 4A, the IR spectrum of a typical Zr-Sil-1 sample B (Si/Zr = 200) in the hydroxyl stretching region shows a strong band at 3720 cm^{-1} which is due to the presence of terminal silanol (Si–OH) groups on the

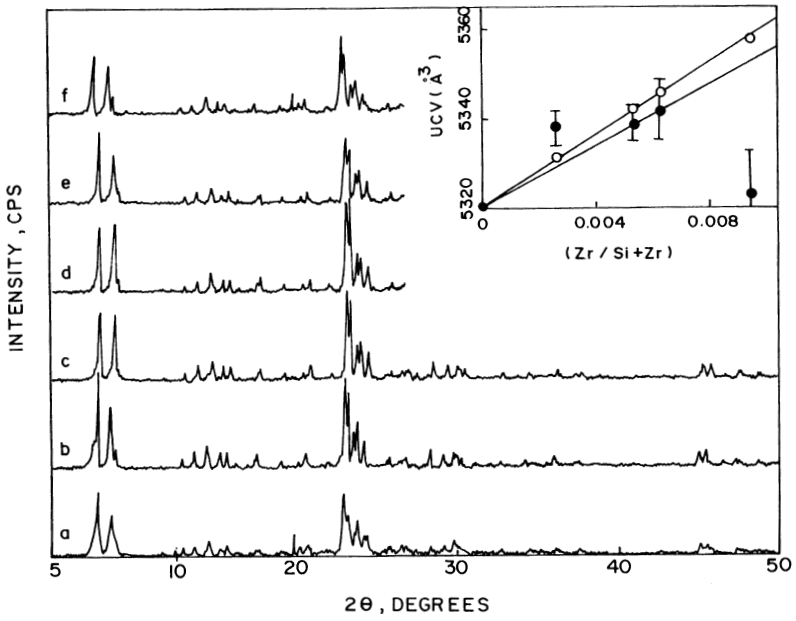

Figure 1. X-ray diffraction profiles of calcined Sil-1 sample (curve a), Zr-Sil-1 samples A to D prepared by hydrothermal synthesis in alkaline medium with Si/Zr molar ratios of 300, 200, 100 and 50 (curves b to e, respectively) and sample E synthesized in HF/CH_3NH_2 medium (curve f). Inset: The variation of unit cell volume with Zr/(Si + Zr) molar ratios in Zr-Sil-1 samples prepared in alkaline medium (V_{uc} (Å^3)), theoretical (○) and experimental (●).

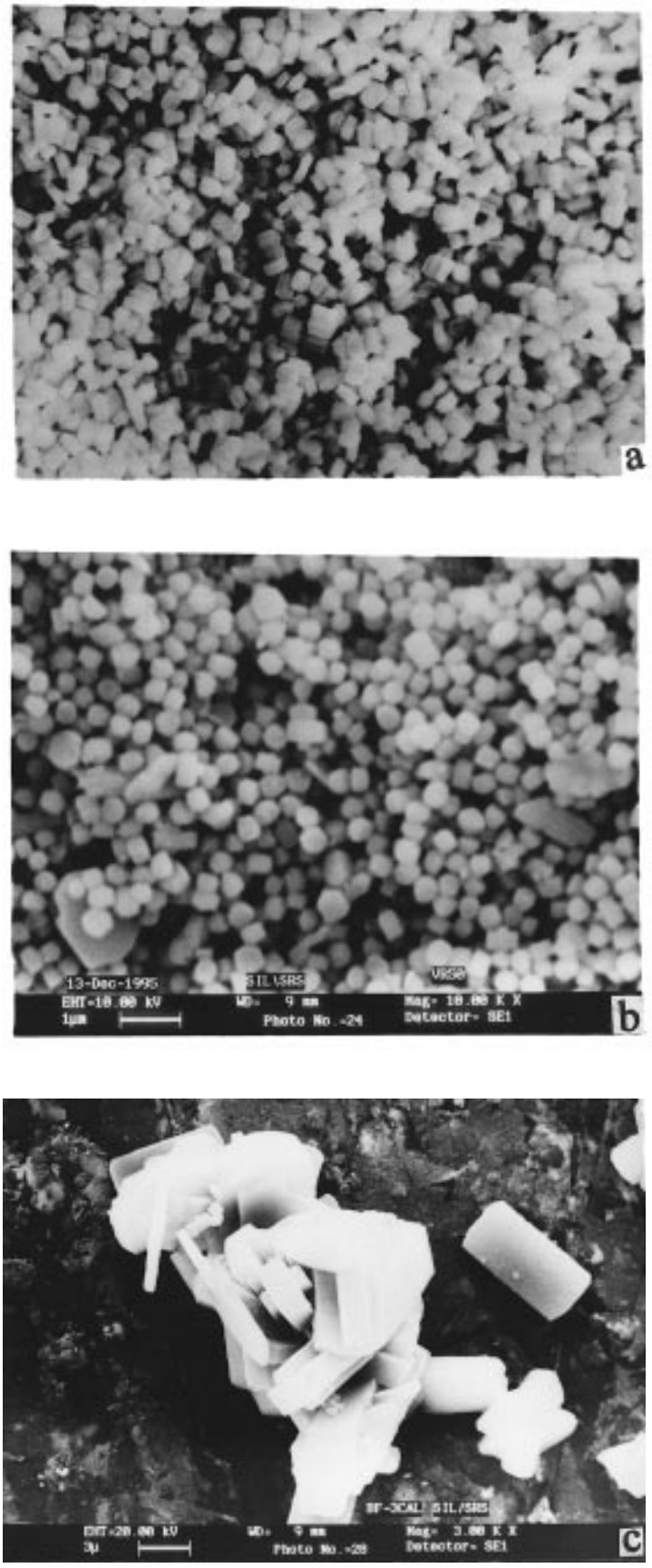

Figure 2. Scanning electron micrographs of Zr-Sil-1 sample A (a), sample D (b), sample F (c) and Sil-1 (d). (Continued on next page.)

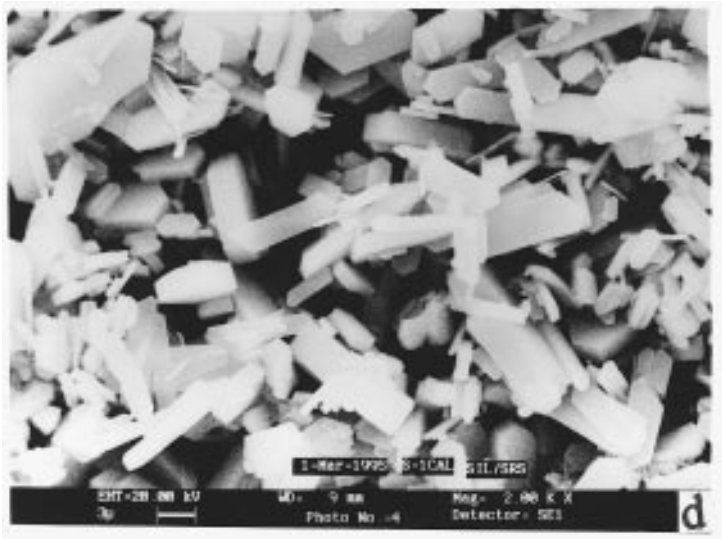

Figure 2. (Continued.)

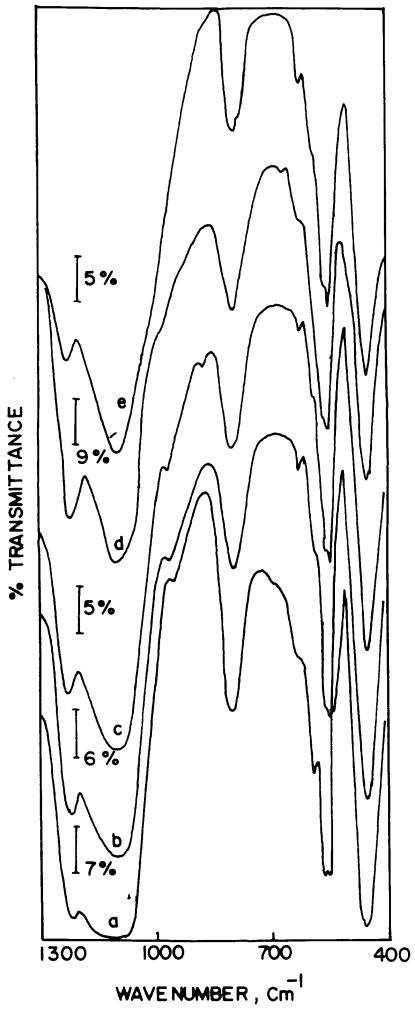

Figure 3. Framework FT-IR spectra of Zr-Sil-1 samples A to D (curves a to d, respectively) and sample F (curve e).

external crystal structure. A broad band of low intensity at 3683 cm^{-1} can be assigned to Zr–OH groups [21]. In figure 4B, the infrared spectra of pyridine (py) adsorbed on sample B after evacuation at 373, 473 and 573 K (curves a to c, respectively) are given. The spectra show strong bands at 1600 and 1450 cm^{-1} due to py coordinately bound to Lewis acid sites (ν_s modes) [22]. A weak band at 1545 cm^{-1} is assigned to the pyridinium ion which provides a measure of Brønsted acid sites. However, the desorption of py at increasing temperatures (> 473 K) resulted in preferential removal of py bound to Brønsted relative to Lewis acid sites. A band of medium intensity at 1490 cm^{-1} due to both the coordinated py and py chemisorbed on protonic acid site (i.e. pyridinium ion) is also observed [23]. Therefore, Zr-silicates with MFI structure appear to be more acidic than Sil-1 and may act as a potential catalyst having most of the desirable characteristics of ZrO_2 [18], and still be a part of the crystalline structure.

The DR UV–Visible spectrum of sample C (Si/Zr = 100) (figure 5, curve b) shows the presence of a characteristic absorption at about 212 nm attributable to charge transfer transitions involving the Zr(IV) (tetrahedral configuration) sites [11]. Zr-Sil-1 sample F, prepared in HF/CH_3NH_2 medium, shows in addition an absorption at 230 nm (curve c) which may be due to Zr(IV) in other coordinations. This absorption is absent in the spectrum of Zr-impregnated Sil-1 sample (curve a). These electronic transitions are clearly distinguishable from those in pure ZrO_2 (monoclinic symmetry) which shows absorption at about 240 and 310 nm (curve d).

The experimental X-ray photoelectron spectrum of sample C, resolved using a gaussian fit, showed two peaks for Zr ($3d_{5/2}$) electron with the binding energies of 174.8 and 183.0 eV (intensity ratio = 1 : 4), respectively and two peaks for Zr ($3d_{3/2}$) electron with binding ener-

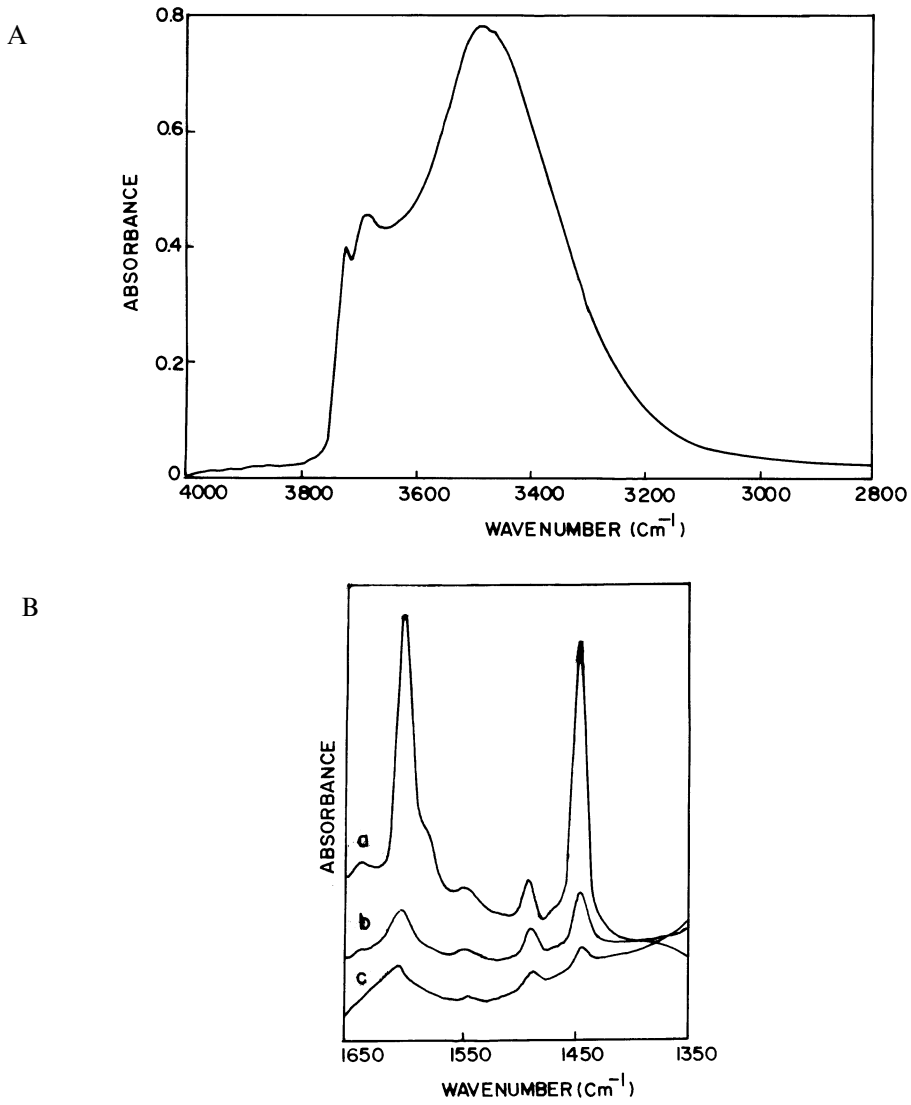

Figure 4. (A) Infrared spectra of Zr-Sil-1 sample B in the hydroxyl stretching region, after evacuation at 673 K. (B) Infrared spectra of pyridine adsorbed on Zr-Sil-1 sample B after evacuation at 373 K (a), 473 K (b) and 573 K (c).

gies of 178.4 and 186.0 eV (intensity ratio = 1 : 3), respectively (figure 6). It confirms the presence of zirconium in the 4+ oxidation state as the main species, in addition to a different coordination which may have Zr=O linkages. This suggestion is supported by XPS studies of $Zr_{76}Fe_{24}$ Metglass [24], wherein similar shifts in the binding energies, due to metallic Zr and ZrO_2 species were observed.

DTA analysis for the samples synthesized in alkaline medium and in HF/CH_3NH_2 medium (samples C and F) showed a strong exothermic peak at 714 and 728 K, respectively. These peaks occur at higher temperatures than that for pure silicalite-1 (663 K). This increase in the temperature of template decomposition can be attributed to lattice distortion, due to the presence of Zr^{4+} ions in the framework [9] and the stronger interaction of template with Zr^{4+} ions in the framework.

The N_2 adsorption isotherms of Zr-Sil-1 samples are characteristic of microporous materials (figure 7). The Sil-1 and sample F (Si/Zr = 100) in HF/CH_3NH_2 medium show a sharp step in the adsorption isotherm which is probably due to the presence of defect sites in the silicalite framework, while Zr-Sil-1 samples A to D in alkaline medium did not show such a step [25]. The micropore areas for samples A to D are in the range of 386–436 m^2/g as against a value of 291 m^2/g obtained for Sil-1 while the samples synthesized in HF/CH_3NH_2 medium showed a decrease in the surface area, due to its bigger particle size (table 1). The amounts of water, *n*-hexane and cyclohexane probe molecules adsorbed on the samples are comparable to that of Sil-1 (table 1). The sorption capacities of Zr-Sil-1 indicate the absence of any pore blockage due to occluded or amorphous material in the microporous structure.

^{29}Si MAS NMR analysis of samples A to G exhibited predominately an intense and broad signal at −113.7 ppm and a shoulder at −115.9 ppm, assigned to Q^4 [$Si(OSi)_4$] species. Since Zr^{4+} is a quadrupole nucleus,

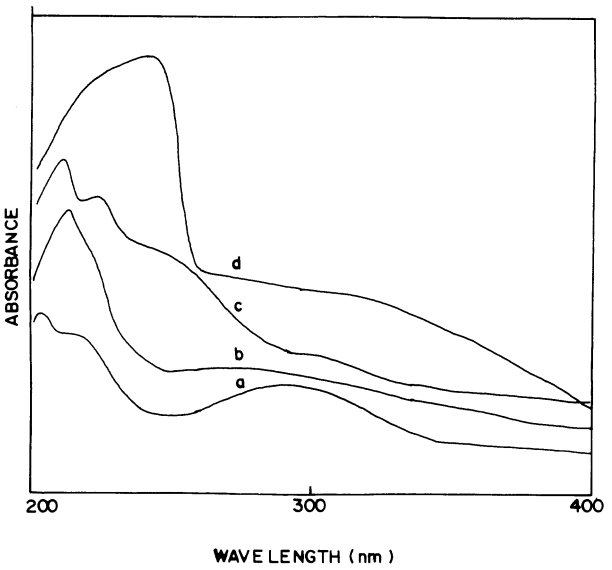

Figure 5. DR UV–Visible spectra of Zr-impregnated Sil-2 (a), Zr-Sil-1 sample C (b), sample E (c) and pure ZrO_2 (d).

it was not possible to get information on the local coordination of Zr^{4+} by MAS NMR experiments. However, the Zr edge EXAFS data will be extremely useful to interpret the local structure and coordination around Zr^{4+} ions. We plan to carry out EXAFS experiments to obtain such data.

3.2. Electronic structure calculation

The adsorption characteristics of pyridine over the

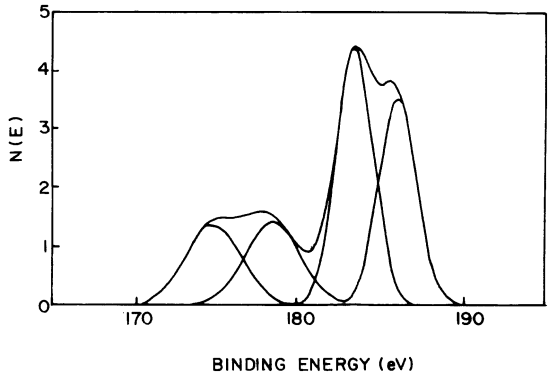

Figure 6. X-ray photoelectron spectra of Zr-Sil-1 sample C.

Brønsted and Lewis acid sites are studied by calculating the interaction of orbitals. The standard extended Hückel molecular orbital (EHMO) method [26] has been applied to derive the electronic structure of the model systems. Although ab initio calculations are desirable to obtain quantitative results, EHMO calculations have been used, since these are a computationally effective technique to derive qualitative information on the ordering of orbitals. Our interest was to compare the extent of splitting in one-electron energy levels after interaction of pyridine with Zr-Sil-1 compared to that splitting in the absence of interaction. The ionization potential and the orbital exponent values for various elements are given in table 2. The parameters for all the row I and row II atoms are default values as in ref. [27], while for Zr, the parameters reported by Tomanek et al. are used [28]. A double-zeta function was used to define the d orbitals of Zr. The

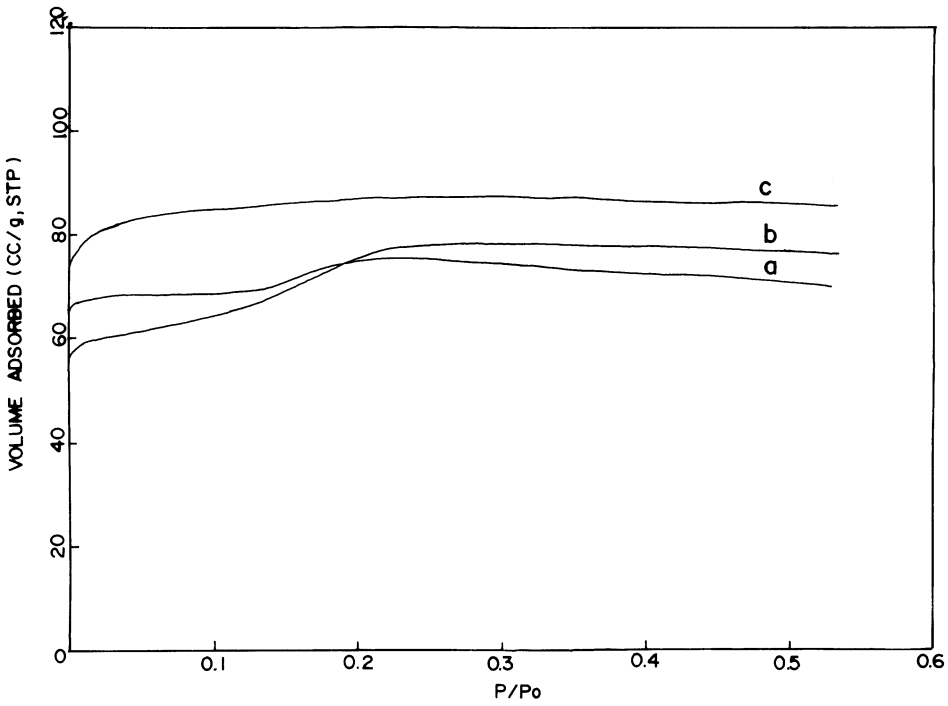

Figure 7. Nitrogen adsorption isotherms at 77 K of Sil-1 (a), Zr-Sil-1 sample F (b) and sample C (c).

Table 2
The parameters used in the EHMO calculations

Orbital		H_{ii} (eV)	ζ_1 [a]	ζ_2 [a]	C_1 [b]	C_2 [b]
H	1s	−13.600	1.300	–	–	–
C	2s	−21.400	1.625	–	–	–
	2p	−11.400	1.625			
N	2s	−26.000	1.950	–	–	–
	2p	−13.400	1.950			
Si	3s	−17.300	1.383	–	–	–
	3p	−9.200	1.383			
Zr	5s	−6.950	1.817			
	5p	−4.930	1.776			
	4d	−8.610	3.835	1.505	0.636	0.593

[a] ζ = orbital exponent.
[b] ζ = contribution factors in the double-ζ functions.

eigenvalues, eigenfunctions, Mulliken overlap populations between atoms and the net charges on atoms were computed with the mean Wolfsberg–Helmholtz formula [27].

Bond distances and bond angles for the pyridine molecule and the cluster models of ZrO_2 are as derived from X-ray structure analysis. Lattice energy calculations coupled with efficient energy minimization procedures have been performed [29]. The minimum energy crystal structures were calculated for ZrO_2 [30] and several dense phases of silicates [29]. These calculations are shown to predict the complex crystal structures correctly, and in fact, the force field parameters are optimized to predict the equilibrium crystal structure. Hence, the geometric parameters of cluster models of ZSM-5 are adopted from the crystal structure reported by Olson et al. [31]. There are 12 crystallographically distinct Si sites in the crystal structure of ZSM-5. The calculations have been carried out on a cluster model $TO_4[T(OH)_3]_4$ (pentamer), where T = Si or Zr, whose suitability to study the properties of zeolites have been evaluated and established elsewhere [32]. In this pentameric cluster model, the central TO_4 tetrahedral unit is linked to four more TO_4 tetrahedra by corner sharing of oxygen atoms. The valencies of the peripheral oxygen atoms are saturated by bonding to hydrogen atoms, whose positions are the same as "T" sites in the crystal lattice. The $SiO_4[Si(OH)_3]_4$ cluster model was used to study the properties of the all siliceous MFI structure. The central "T" site was substituted by Zr, while the four peripheral $T(OH)_3$ groups are $Si(OH)_3$, thus leading to a cluster model of $ZrO_4[Si(OH)_3]_4$. This model shown in figures 8a and 8b is used to represent the isomorphously substituted Zr^{4+} in the place of Si^{4+} ions in the ZSM-5 structure.

The ease of this substitution at the 12 crystallographically distinct sites is calculated as substitution energy values. The substitution energy at different sites had similar values with slight preference for Zr^{4+} substitution at sites 2 and 12, where the Si–O distances are the largest and Si–O–Si bond angle values are the smallest.

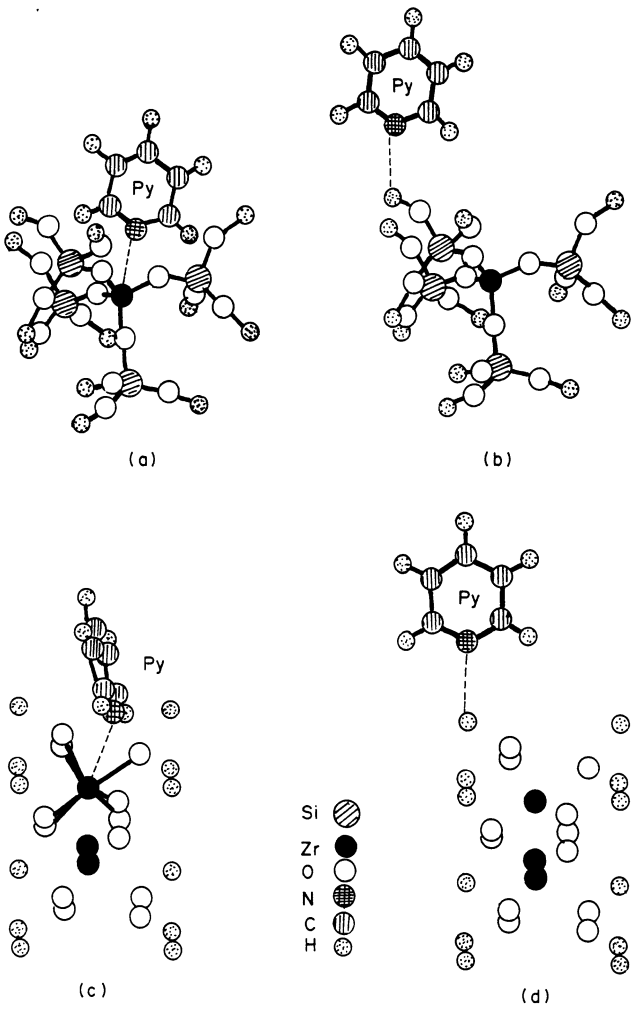

Figure 8. The cluster models used in the EHMO calculations. A typical pentameric cluster model centered at the T2 site of the MFI structure, wherein pyridine (py) is coordinately bound to a Lewis site (a) (binding energy = −4.37 eV) and bound to a Brønsted site (b) as pyridinium ion (binding energy = −1.79 eV) is shown. A typical cluster model representing the monoclinic phase of ZrO_2, wherein py is coordinately bound to Lewis acid site (c) (binding energy = −2.03 eV) and bound to Brønsted site (d) as pyridinium ion (binding energy = −1.88 eV) is shown. In the cluster models (c) and (d), only the atom positions are shown. The seven-coordination of zirconium is highlighted in cluster model (c).

The sites 2 and 12 are common to both straight and sinusoidal channels. The sites 8 and 11 are the least preferred sites for the substitution of Zr^{4+} ions. The sites 8 and 11 never occur in the sinusoidal channel but occur only in the straight channel and hence statistical distribution of Zr in the sinusoidal channel is expected to be higher. However, the ordering of the molecular orbitals remains the same independent of the small variations in the geometry of different crystallographic sites. The energy minimization procedures performed with interatomic potential of central-force ionic models lead to uniform geometries for all the cluster models representing several crystallographic sites. Thus these results bring out the fact that the nature of the acid sites and their interaction

with basic molecules such as pyridine are not dependent on the crystallographic location of Zr^{4+} ions in the zeolite lattice.

The interaction of pyridine with Zr^{4+} in the monoclinic phase of ZrO_2 was calculated by analyzing the electronic structure of suitable cluster models shown in figures 8c and 8d. The coordination of Zr^{4+} ions in ZrO_2 is seven-fold while it is four-fold (tetrahedral symmetry) in the Zr-Sil-1. The net charges on the atoms are in correspondence with this as given by Mulliken population values. The Lewis acidity of the isolated Zr surrounded by SiO_4 tetrahedra in Zr-Sil-1 sample is stronger than that of Zr in ZrO_2 lattice. This trend is predicted in the binding energy of pyridine given in figure 8. The bonding of pyridine to Zr in ZrO_2 is also hindered due to its relatively crowded coordinations compared to the situation in Zr-Sil-1. The pyridinium ion formation on the surface –Zr–OH groups in ZrO_2 and with the silanol groups in the Zr-Sil-1 sample was studied. The binding energy of pyridine with surface hydroxyl groups (figures 8b and 8d) is less compared to the case of binding energy of pyridine when it is coordinated to Zr^{4+} ions (figures 8a and 8c). In the former case, the interaction of the lone pair of pyridine is with the hydrogen 1s orbital, while in the latter case it is with the Zr 4d orbitals. Although the LUMO band is a composite of H 1s and Zr 4d orbitals, the low-lying orbitals get more contribution from the 4d orbitals of Zr. The dependence of the stabilization of 4d orbitals on the coordination is also brought out from the results of the calculations on the cluster models shown in figures 8a and 8b. Stabilization of e_g orbitals in the tetrahedral coordinations is the cause of the stronger Lewis acidity of Zr- Sil-1 samples.

3.3. Catalytic reaction

Catalytic reactions such as hydroxylation of phenol provide information about the framework location of substituted heteroatoms in the silicalite structure [33,34]. Hydroxylation of phenol over Zr-Sil-1 samples was carried out using aqueous H_2O_2 as an oxidizing agent. The samples showed 34 wt% H_2O_2 selectivity with turnover number (TON) of 112 (table 3). A catechol (CAT) to hydroquinone (HQ) ratio of 1.0–1.4 for the Zr-Sil-1 samples indicates a certain degree of shape selectivity. A CAT/HQ ratio of 0.9–1.3 has been reported for the titanium silicates and vanadium silicates [35]. These results indicate that, in addition to being well dispersed, the Zr^{4+} ions are probably located within the channels of the MFI structure as active sites. The catalyst can be regenerated without significant loss in activity. In order to check the catalytic behaviour of Zr-Sil-1, blank reactions were carried out on Zr-impregnated Sil-1, amorphous Zr-silica and Sil-1 samples under identical conditions and were found to have negligible activity in the reaction. Apparently, only those zirconium ions present in the silicalite framework are active in the reaction. The samples synthesized in HF/CH_3NH_2 medium showed negligible catalytic activity (table 3, sample F) but the product selectivity (CAT/HQ = 2) was different as compared to blank reactions, probably due to their bigger particle size.

4. Conclusions

The synthesis of zirconium silicates with different Si/Zr ratios by two different synthetic routes is reported. The dependence of physico-chemical, structural and catalytic properties of samples prepared by two routes are discussed. Incorporation of Zr^{4+} in the place of Si^{4+} in MFI framework causes an increase in unit cell volume. There seems to be an upper limit for the extent of incorporation of Zr^{4+} in the framework which is 0.6 Zr/unit cell (unit cell expansion of 5321–5342 $Å^3$). Absence of amorphous matter is confirmed by XRD and SEM studies. The framework IR spectra showed the presence of Si–O–Zr linkages as well as Zr=O type species. The IR

Table 3
Hydroxylation of phenol [a]

Catalyst	TON [c]	H_2O_2 sel.	Product distribution [b] (wt%)		
			PBQ	CAT	HQ
Zr/Sil-1 [d]	–	3.0	38.5	58.2	3.3
amorphous Zr-silica	–	2.4	35.5	62.6	1.9
Sil-1	–	8.5	51.7	47.4	0.9
Zr-Sil-1(200) [e]	98.6	24.6	1.3	49.3	49.4
Zr-Sil-1(100) [e]	112.0	33.5	0.8	58.2	41.0
Zr-Sil-1(50) [e]	62.2	27.9	1.3	43.3	54.9
Zr-Sil-1(100) [e,f]	8.3	2.6	8.2	61.9	29.9

[a] Reaction conditions: catalyst = 0.5 g; solvent = 10 g; phenol/H_2O_2 (mol) = 3; reaction duration = 10 h; temperature = 353 K.
[b] For formation of parabenzoquinone (PBQ), catechol (CAT) and hydroquinone (HQ), excluding tar.
[c] Turnover number = moles of phenol converted per mole of Zr atom.
[d] Zr-impregnated Sil-1, for similar amount of Zr as in the case of Zr-Sil-1(158).
[e] Si/Zr molar input ratio in parentheses.
[f] Sample synthesized in HF/CH_3NH_2 medium.

spectra in the hydroxyl stretching region showed the presence of Si–OH and Zr–OH groups on the surface. The IR spectra of the adsorbed pyridine showed the presence of strong Lewis and weak Brønsted acid sites. The pyridinium ions at the Brønsted acid sites are weakly bound in correspondence with the Si–OH and Zr–OH type weak Brønsted acid sites predicted earlier. Further, a characteristic absorption at 212 nm in the UV–Visible spectrum and the two peaks with binding energy values about 185.0 eV for $3d_{5/2}$ and $3d_{3/2}$ in the XPS spectrum support the presence of Zr in tetrahedral coordination. The catalytic activity for the hydroxylation of phenol is far superior for the samples prepared in alkaline medium than those prepared in HF/CH_3NH_2 medium. The product selectivity obtained in the reaction indicates the presence of Zr^{4+} in the channels, rather than on the surface. The ordering and shift in the molecular orbitals are not significantly different for monoclinic zirconia and orthorhombic zirconium silicate structures, as derived from the cluster calculations. However, the binding energy of pyridine is significantly higher when it is coordinated to zirconium in comparison to the situation when it is forming pyridinium ion with surface hydroxyl groups.

Acknowledgement

We acknowledge the help extended by Dr. S. Badrinarayanan (XPS), Dr. S.R. Sainkar (SEM) and TCR Engg. (ICP analysis). BR thanks CSIR, New Delhi for a senior research fellowship.

References

[1] M. Taramasso, G. Perego and G. Bellusi, US Patent 4,410,501 (1983).
[2] G. Bellussi, A. Carati, M.G. Clerici, A. Esposito, R. Millini and F. Buonomo, Belg. Patent 1,001,038 (1989).
[3] N.K. Mal, V. Ramaswamy, S. Ganapathy and A.V. Ramaswamy, J. Chem. Soc. Chem. Commun. (1994) 1933.
[4] N.K. Mal, V. Ramaswamy, S. Ganapathy and A.V. Ramaswamy, Appl. Catal. A 125 (1995) 233.
[5] D.A. Young, US Patents 3,329,480, 3,329,481 (1967).
[6] B. Herbert, L. Heinz, L. Ernst Ingo and W. Friedrich, EP 77,523 A2 (27 April 1983).
[7] W. Pang, L. Yu and Y. Wu, Chem. J. Chinese Univ. 7 (1986) 63.
[8] M.K. Dongare, P. Singh, P. Moghe and P. Ratnasamy, Zeolites 11 (1991) 690.
[9] R. Fricke, H. Kosslick, V.A.Tuan, I. Grohmann, W. Pilz, W. Storek and G. Walther, Stud. Surf. Sci. Catal. 83 (1994) 57.
[10] M. Costantini, J.L. Guth, A. Lopez and J.M. Popa, EP 466,545 (1990).
[11] G.R.Wang, X.Q. Wang, X.S. Wang and S.X. Yu, Stud. Surf. Sci. Catal. 83 (1994) 67.
[12] R.D. Shannon, Acta Cryst. A 32 (1976) 751.
[13] R. Szostak, *Molecular Sieves: Principles of Synthesis and Identification* (Van Nostrand Reinhold, New York, 1989) p. 317.
[14] P.J. Dirken, M.E. Smith and H.J. Whitfield, J. Phys. Chem. 99 (1995) 395.
[15] D. Scarano, A. Zecchina, S. Bordiga, F. Geobaldo, G. Spoto, G. Petrini, G. Leofanti, M. Padovan and G. Tozzola, J. Phys. Chem. 89 (1993) 4123.
[16] Z. Liu and R.L. Davis, J. Phys. Chem. 98 (1994) 1253.
[17] J.R. Sohn, H.J. Jang, E.H. Park and S.E. Park, J. Mol. Catal. 93 (1994) 149.
[18] Z. Dang, B.G. Anderson, Y. Amenomiya and B.A. Morrow, J. Phys. Chem. 99 (1995) 14437.
[19] K. Dehnicke and J. Weidlein, Angew. Chem. Int. Ed. 5 (1966) 1041.
[20] D.C. Bradly and P. Thronton, *Comprehensive Inorganic Chemistry*, Vol. 3 (Pregamon Press, Oxford, 1973).
[21] T. Yamaguchi, Catal. Today 20 (1994) 199.
[22] C. Morterra and G. Cerrato, Langmuir 6 (1990) 1810.
[23] K. Ebitani, H. Hattori and K. Tanabe, Langmuir 6 (1990) 1743.
[24] S. Sinha, S. Badrinarayananan and A.P.B. Sinha, J. Less Common Metals 125 (1986) 85.
[25] G.L. Marra, G. Tozzola, G. Leofanti, M. Padovan, G. Petrini, F. Genoni, B. Venturelli, A. Zecchina, S. Bordiga and G. Ricchiardi, Stud. Surf. Sci. Catal. 84 (1994) 559.
[26] R. Hoffmann, J. Chem. Phys. 39 (1963) 1397.
[27] C.J. Ballhausen and H.B. Gray, *Molecular Orbital Theory* (Benjamin, New York, 1965).
[28] D. Tomanek, R. Hauert, P. Oelhafen, R. Schlögl and H.J. Guntherodt, Surf. Sci. 160 (1985) L 493.
[29] C.R.A. Catlow, P.A. Cox, R.A. Jackson, S.C. Parker, G.D. Price, S.M. Tomlinson and R. Vetrivel, Mol. Simulation 3 (1989) 49.
[30] V. Butler, C.R.A. Catlow, B.E.F. Fender and J.H. Harding, Solid State Ionics 8 (1983) 109.
[31] D.H. Olson, G.T. Kokotailo, S.L. Lawton and W.M. Meier, J. Phys. Chem. 85 (1981) 2238.
[32] A. Chatterjee and R. Vetrivel, Microporous Mater. 3 (1994) 211.
[33] A. Esposito, C. Neri, F. Buonomo and M. Taramasso, UK patent 2,116,974 (1983).
[34] G. Perego, G. Bellusi, C. Corno, M. Taramasso, F. Buonomo and A. Esposito, Stud. Surf. Sci. Catal. 28 (1986) 129.
[35] A.V. Ramaswamy and S. Sivasanker, Catal. Lett. 22 (1993) 239.